MATERIALS SCIENCE

Molecular engineered conjugated polymer with high thermal conductivity

Yanfei Xu,[1]* Xiaoxue Wang,[2]* Jiawei Zhou,[1] Bai Song,[1] Zhang Jiang,[3] Elizabeth M. Y. Lee,[2] Samuel Huberman,[1] Karen K. Gleason,[2]† Gang Chen[1]†

Traditional polymers are both electrically and thermally insulating. The development of electrically conductive polymers has led to novel applications such as flexible displays, solar cells, and wearable biosensors. As in the case of electrically conductive polymers, the development of polymers with high thermal conductivity would open up a range of applications in next-generation electronic, optoelectronic, and energy devices. Current research has so far been limited to engineering polymers either by strong intramolecular interactions, which enable efficient phonon transport along the polymer chains, or by strong intermolecular interactions, which enable efficient phonon transport between the polymer chains. However, it has not been possible until now to engineer both interactions simultaneously. We report the first realization of high thermal conductivity in the thin film of a conjugated polymer, poly(3-hexylthiophene), via bottom-up oxidative chemical vapor deposition (oCVD), taking advantage of both strong C=C covalent bonding along the extended polymer chain and strong π-π stacking noncovalent interactions between chains. We confirm the presence of both types of interactions by systematic structural characterization, achieving a near–room temperature thermal conductivity of 2.2 W/m·K, which is 10 times higher than that of conventional polymers. With the solvent-free oCVD technique, it is now possible to grow polymer films conformally on a variety of substrates as lightweight, flexible heat conductors that are also electrically insulating and resistant to corrosion.

INTRODUCTION

Polymers have infiltrated almost every aspect of modern technology (*1*). Wearable sensors, soft robotics, and three-dimensional printing are all examples of advanced technologies enabled by flexible and lightweight polymers (*1*). However, polymers are still primarily regarded as heat insulators (*2*, *3*), and the low thermal conductivity (~0.2 W/m·K) hinders their adoption in a variety of applications. Until now, metals and ceramics remain the dominant heat conductors.

The low thermal conductivity of polymers is generally considered a result of structural disorders and weak molecular interactions (*2*, *3*). By systematically improving the alignment of molecular chains through stretching (*4*–*9*), template-assisted growth (*10*, *11*), surface grafting (*12*), etc., polymers with orders-of-magnitude higher thermal conductivities along the chain direction have been reported (*4*–*11*). More specifically, a thermal conductivity over 100 W/m·K has been reported for ultradrawn polyethylene nanofibers (*7*); a thermal conductivity of ~4.4 W/m·K has been achieved through nanoscale template-assisted electropolymerization of polythiophene nanofibers (*10*); and a thermal conductivity greater than 2 W/m·K has been measured for surface-grafted polymer brushes (*12*). However, these approaches either pose scalability challenges for practical applications or are limited to the anisotropic scenario of high thermal conductivity along the chain direction and low thermal conductivity between the chains (*13*). The problem of poor interchain thermal transport is due to the weak van der Waals (vdW) force between the chains (*3*). Recently, intermolecular hydrogen bonding has been exploited as a means to go beyond vdW interactions (*14*–*16*), leading to a significantly increased isotropic thermal conductivity of ~1.5 W/m·K in water-soluble polymers (*15*). Alternatively, thermal conductivity has also been increased to ~1.2 W/m·K in electrostatically engineered amorphous polymers (*17*). However, these approaches either require a specific pH environment or pose challenges in terms of stability and reliability for practical applications (*14*). To date, it remains a long-standing challenge to enhance the thermal conductivity of polymers by simultaneously engineering the intramolecular and intermolecular interactions, which is key to realizing efficient isotropic thermal transport.

Conjugated polymers are potential candidates for good thermal conductors, considering both the rigid conjugated backbone and the strong intermolecular π-π stacking interactions. Carbon-carbon single bonds (C–C, ~347 kJ/mol) (*18*) are prevalent in diamond (~2000 W/m·K) (*19*) and stretched polyethylene (~104 W/m·K) (*7*) and are key to their ultrahigh thermal conductivities. Compared to C–C single bonds, conjugated carbon-carbon double bonds (C=C, ~610 kJ/mol) are nearly twice as strong and thus are expected to dramatically improve phonon transport along the polymer chains (*20*). Furthermore, the π-π stacking interaction between the chains is approximately 10 to 100 times stronger than the weak vdW interactions (vdW ~0.4 to 4 kJ/mol) (*21*), which could substantially enhance phonon transport across the chains. Traditional conjugated polymers are characterized by low thermal conductivities (~0.2 W/m·K) similar to nonconjugated polymers. Researchers hypothesize that such low thermal conductivity is due to strong phonon scatterings by chain distortions, entanglements, and so on (*3*, *20*). To realize the full potential of conjugated polymers, the remaining critical challenge is how to precisely control the conformation of the planar conjugated backbones together with the interchain π-π stacking at the molecular level.

Here, we report thermally conductive conjugated poly(3-hexylthiophene) (P3HT) thin film fabricated using oxidative chemical vapor deposition (oCVD). This all-dry vapor phase technique directly synthesizes a polymeric thin film using monomers via step growth polymerization (Fig. 1 and fig. S1). The oCVD approach offers unique advantages for integrating polymer films into various devices (*22*). For example, by avoiding the use of solvents and their undesirable surface tension–driven effects such as dewetting, it enables conformal coating of complex geometries. Furthermore, it is scalable to a large area and can be carried out at low temperatures on electrically insulating substrates, allowing virtually any surface to

[1]Department of Mechanical Engineering, Massachusetts Institute of Technology, Cambridge, MA 02139, USA. [2]Department of Chemical Engineering, Massachusetts Institute of Technology, Cambridge, MA 02139, USA. [3]Advanced Photon Source, Argonne National Laboratory, Argonne, IL 60439, USA.
*These authors contributed equally to this work.
†Corresponding author. Email: kkg@mit.edu (K.K.G.); gchen2@mit.edu (G.C.)

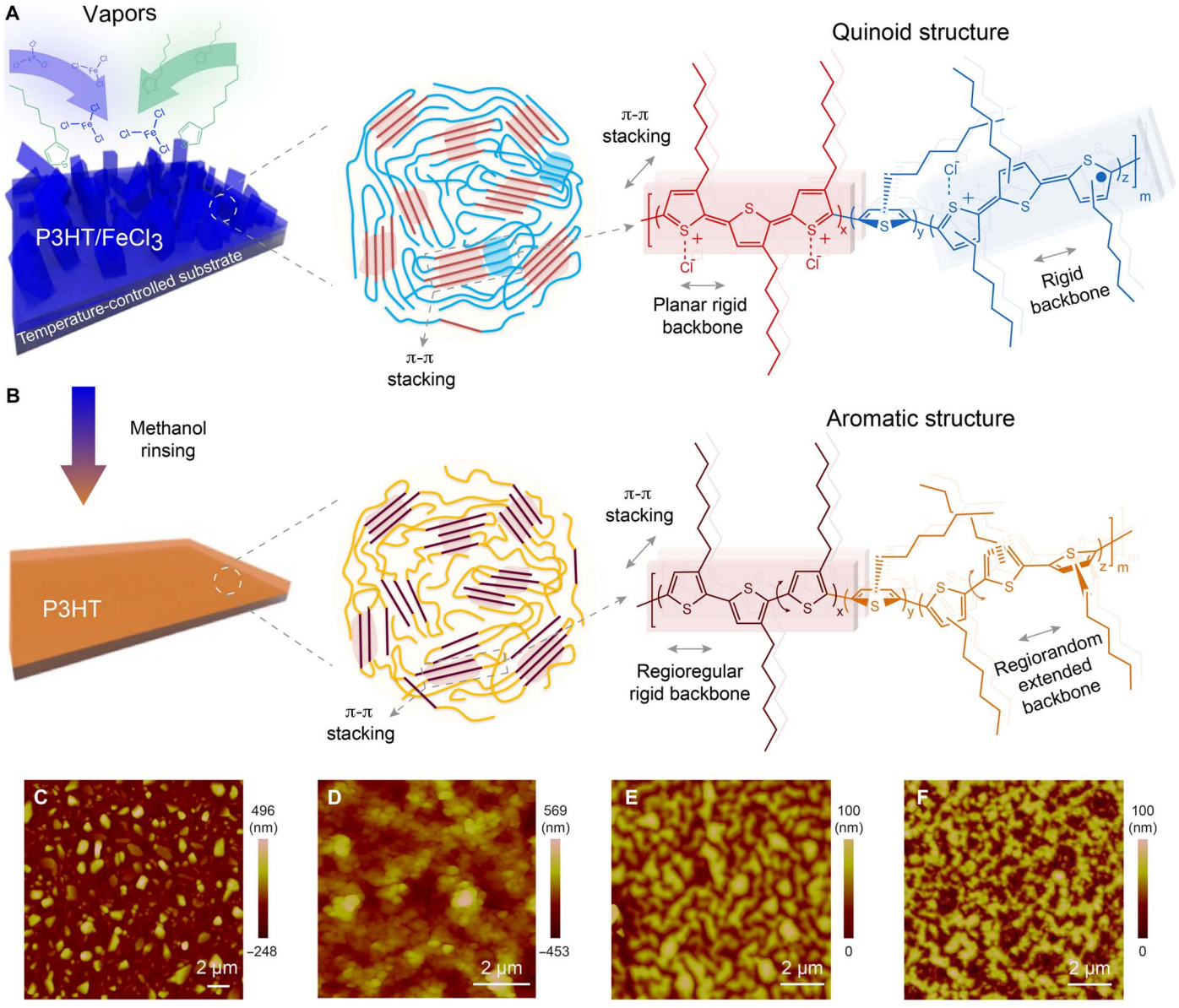

Fig. 1. oCVD synthesis process, molecular structure, and film morphology. (**A**) P3HT/$FeCl_3$ thin film. Left: Initialization of the film growth with adsorbed monomer (3-hexylthiophene) and oxidant ($FeCl_3$) from their vapor phase and the continuous growth of the nanorod-like structures. Middle: Schematic of the microstructure of the doped P3HT film; ordered chain grains (red and blue shades) are π-π stacking assemblies, whereas disordered chain grains have rigid backbones with suppressed distortions. Right: Extended chains in quinoid form grown on $FeCl_3$. The (bi)polarons are present in the doped P3HT backbone. (**B**) P3HT thin film. Methanol rinsing removes excess oxidant and de-dopes (reducing) the P3HT backbone. Middle: Schematic of the microstructure of the de-doped P3HT film showing ordered chain assemblies via π-π stacking (red shades) and extended chains with suppressed distortions, which originate from the quinoid structures in (A). Unlike coiled and entangled chains in typical polymers (fig. S2A), the extended chains of the de-doped P3HT are obtained (fig. S2B). (**C** to **F**) Film morphology characterized by tapping-mode AFM. (C) P3HT/$FeCl_3$ grown at 45°C (40-min polymerization). (D) P3HT/$FeCl_3$ grown at 85°C (40-min polymerization). The surface roughness (Ra) for both 45°C- and 85°C-grown P3HT/$FeCl_3$ is more than 80 nm. (E) For the 45°C-grown P3HT, the roughness is ~13.8 nm. (F) For the 85°C-grown P3HT, the roughness is ~14.5 nm.

be coated. Here, we show that ordered structures with rigid backbones can be produced by oCVD with stacking in the transverse direction via π-π interactions (Fig. 1). By simultaneously harnessing the strong conjugated bonds along polymer chains and the π-π interactions between them, we obtain a record-high thermal conductivity of 2.2 W/m·K near room temperature. As a model polymer for organic electronics (*23*), including solar cells and field-effect transistors, P3HT with high thermal conductivity may offer unique opportunities for improved heat dissipation.

RESULTS

Figure 1 shows our design concept and synthesis strategy. The oCVD process includes the following steps: (i) introduction of vaporized monomers and oxidants into a vacuum chamber, (ii) physical adsorption of monomers and oxidants onto cooled substrates, and (iii) step growth and oxidative coupling polymerization of adsorbed monomers (fig. S1). Notably, oCVD-grown polymer films generally have high chemical purity with no residues as compared to solution-based processes because

the vapor deposition process is inherently free of solvents and additives (*22*, *24*, *25*). Here, the P3HT thin films are grown at two different substrate temperatures (45° and 85°C) (*22*). Because the adsorption of the monomers (3-hexylthiophene) and oxidants ($FeCl_3$) onto the surface limits the polymerization rate, the low temperature substrates promote adsorption and lead to rapid polymerization (*26*). More crucially, the oxidants on the substrate also serve as hosting templates for polymer chain growth (Fig. 1A and fig. S1), and the excessive oxidants can heavily oxidatively dope the polymer backbone during the chain growth process, significantly stabilizing the quinoid structure—a conjugated segment with rigid double bonds linking two thiophene rings (fig. S1E, left) instead of the rotatable single bond (fig. S1E, right)—at the molecular level. The presence of a quinoid structure, as confirmed by ultraviolet-visible–near-infrared spectroscopy (UV-vis-NIR) later in this work, is important for obtaining high thermal conductivity because of its high planarity arising from double bonds and extended conjugation (*26*). Such planarity enables regular self-assembly of multiple chains through π-π stacking force (Fig. 1, A and B, middle and right). Thus, P3HT with a rigid, planar conjugated backbone and strong interchain π-π interactions is realized simultaneously during the polymerization process (Fig. 1B) (*23*). After a thorough methanol rinsing process, the backbone is de-doped (reduced) and intrinsic P3HT (neutral state) with an extended aromatic chain is obtained (fig. S2B), as compared to the usually coiled and entangled chains in polymers (fig. S2A). Below, we use "P3HT" to represent the intrinsic P3HT and "P3HT/$FeCl_3$" for the mixed system of doped P3HT and $FeCl_3$.

Atomic force microscopy (AFM) reveals the unique nanorod-like growth mechanism of oCVD. After 10 min of deposition, island growth is observed. The 45°C-grown P3HT/$FeCl_3$ has larger islands than the 85°C-grown P3HT/$FeCl_3$ (fig. S3, A and B). After 40 min, the 45°C-grown P3HT/$FeCl_3$ displays highly ordered nanorod-like features, whereas the 85°C-grown P3HT/$FeCl_3$ is porous (Fig. 1, C and D). Modest electrical conductivities of 4.35 ± 0.44 S/cm and 0.001 ± 0.0004 S/cm are measured for the 45°C- and 85°C-grown P3HT/$FeCl_3$, respectively. The higher electrical conductivity of 45°C-grown P3HT/$FeCl_3$ is hypothesized to originate from the longer conjugation length in the quinoid structure along the ordered chain (*27*). Both P3HT films display significant morphology changes after de-doping (Fig. 1, E and F). The surface roughness (Ra) of the 45°C- and 85°C-grown P3HT films is ~13.8 nm and 14.5 nm, respectively. The absence of residue in the intrinsic P3HT confirms its high chemical purity (fig. S3C), and the grown P3HT film thickness is ~160 nm (fig. S3E; see the "Thickness measurement" section in the Supplementary Materials).

To investigate the thermal properties of P3HT, we performed thermal conductivity measurement using time-domain thermoreflectance (TDTR) (fig. S6; see the "Thermal conductivity measurement" and "Notes on TDTR experimental sensitivity and uncertainty" sections in the Supplementary Materials) (*28*, *29*). The oCVD sample is coated with an approximately 100-nm-thick layer of aluminum (Al) transducer via electron beam evaporation. The pump pulse heats up the Al layer, whereas the probe pulse monitors the decay of surface temperature. From the measured surface temperature decay, the effective thermal conductivity (k_{eff}) in the thickness direction (perpendicular to the substrate) can be obtained by fitting to a multilayer Fourier heat conduction model (*29*). In Fig. 2, we show representative thermal conductivity data of P3HT films grown on glass substrates. The 45°C-grown P3HT film has a thermal conductivity 10 times higher than that of the 85°C-grown P3HT film. The thermal conductivity of the 45°C-grown P3HT increases from ~1.3 W/m·K at 200 K to ~2.2 W/m·K at 280 K and then flattens out around 300 K (Fig. 2). This trend potentially indicates the "polycrystalline" nature of the P3HT film. As revealed later by x-ray scattering analysis, the 45°C-grown P3HT has both crystalline (well-organized) and amorphous regions. The crystalline regions (facilitated by the quinoid structure) are similar to the grains in typical inorganic polycrystalline samples, whereas the amorphous regions resemble interfaces between crystalline grains. At low temperatures, phonon propagation inside the crystalline region is limited by the scattering at interfaces, and thermal conductivity increases with increasing phonon population. At higher temperatures, however, the intrinsic phonon scattering becomes dominant, which could lead to decreasing thermal conductivity as temperature is further increased. Therefore, the observed trend of temperature-dependent thermal conductivity may indicate the transition between these two regimes.

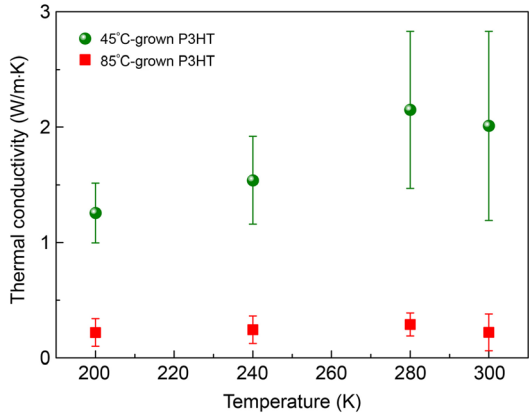

Fig. 2. Measured thermal conductivity using TDTR. Temperature-dependent thermal conductivity of P3HT films grown on glass substrates. The green spheres were measured from a 45°C-grown P3HT film and show a thermal conductivity as high as 2.2 W/m·K. The averages of 20 transient thermoreflectance measurements at 9-, 6-, and 3-MHz modulation frequencies are plotted. The error bars mark 2 SDs (95% confidence interval). All the samples measured were intrinsic P3HT (de-doped), rather than P3HT/$FeCl_3$ (doped).

Even in the presence of an amorphous phase, the thermal conductivity of the 45°C-grown P3HT perpendicular to the interface is 10 times higher than that of typical polymers (*11*). This thermal conductivity enhancement could originate from the quinoid structure, which suppresses chain distortion during the growth process (Fig. 1A and fig. S1E). Compared to the coiled and entangled chains in typical polymers (fig. S2A), the extended and largely ordered backbones facilitate phonon transport along the chains (fig. S2B).

To confirm the presence of the quinoid structure, we performed UV-vis-NIR spectra of 45°C- and 85°C-grown P3HT/$FeCl_3$ (Fig. 3A). Typical absorption bands of (bi)polarons are clearly observed at 700 to 900 nm and 1800 nm, which confirmed that (bi)polarons are present (*23*). We can thus conclude that quinoid structures, which suppress the chain distortions, are formed in the chain growth process. Compared to the 45°C-grown P3HT/$FeCl_3$, the 85°C-grown P3HT/$FeCl_3$ exhibits (bi)polaron peaks that are blue-shifted. This blue shift may be due to more irregular or shorter polymer chains (*23*).

The dynamics of thermal transport in polymers is complex because of many factors including polymer chain structure and microstructure morphology. To explore the relationship between structure and thermal property, we first study the conjugation length of the P3HT molecules and the degree of ordering in P3HT thin films by UV-vis absorption spectroscopy (*30*). Normalized UV-vis absorption spectra of the

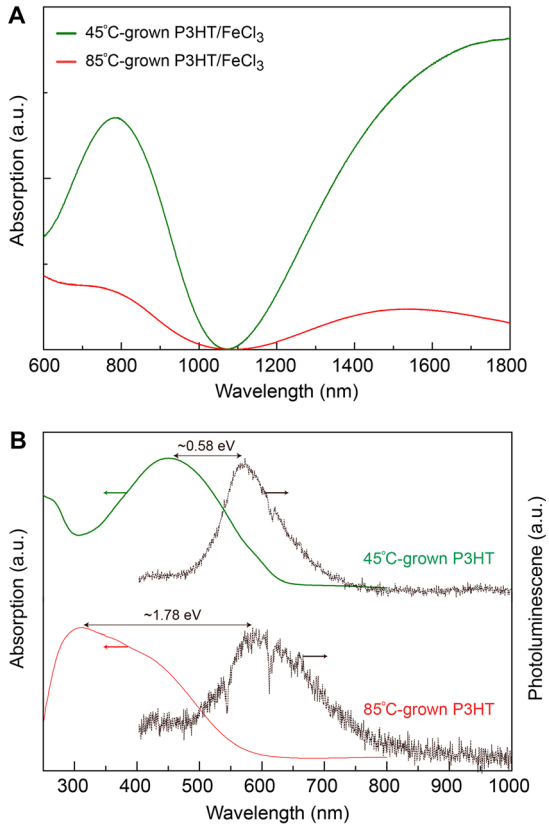

Fig. 3. Absorption and emission spectra. (**A**) UV-vis-NIR spectra of the 45°C- and 85°C-grown P3HT/$FeCl_3$ films on glass substrates. Typical absorption bands of the (bi)polarons are observed at 700 to 900 nm and 1800 nm, suggesting that quinoid structures are formed during polymerization (Fig. 1A). The (bi)polaron peaks in the 85°C-grown sample are blue-shifted. a.u., arbitrary units. (**B**) Absorption and emission spectra of intrinsic P3HT films on glass substrates. In the absorption spectra, the absorbance peak occurs at a longer wavelength for the 45°C-grown P3HT sample, suggesting a longer conjugation length than in the 85°C-grown P3HT. In the photoluminescence spectra, a smaller Stokes shift in the 45°C-grown P3HT film suggests less conformational strain in the ground state than in the 85°C-grown P3HT. All spectral intensities have been normalized with respect to their peaks corresponding to the π-π* transition.

45°C- and 85°C-grown P3HT show maximum absorption (λ_{max}) at ~451 and 311 nm, respectively (Fig. 3B). This λ_{max} is assigned to the π-π* transition (*31*). A larger λ_{max} is observed in the 45°C-grown sample than in the 85°C-grown sample. This is indicative of a longer conjugation length and more coplanar thiophene rings in the 45°C-grown sample (*32*), which is consistent with the higher electrical conductivity in the 45°C-grown P3HT/$FeCl_3$. Longer conjugation length can improve intrachain thermal transport (*31*, *33*). Meanwhile, π-extended planar backbones enable self-assembly of regioregular sections to form crystalline regions. This is confirmed by x-ray scattering analysis (Fig. 4 and fig. S3D). Such ordered regioregular sections connected by the extended chains crucially contribute to the high thermal conductivity in the 45°C-grown P3HT film (Fig. 1B and fig. S2).

To further investigate thermal conductivity affected by regiorandom backbones (fig. S1D), we performed photoluminescence spectroscopy using laser excitation at 365 nm (Fig. 3B). The maximum emission wavelengths for the 45°C- and 85°C-grown P3HT are about the same (~580 nm). Stokes shifts for the 45°C- and 85°C-grown P3HT are ~0.58 eV and ~1.78 eV, respectively. The Stokes shift of the emission spectra compared to absorption spectra indicates atomic relaxation upon excitation (*23*, *34*). When electrons are excited into higher-level states via photoabsorption, the local polymer conformation adopts a more regular structure to stabilize the excited state, which is then followed by the red-shifted emission (*23*). The smaller Stokes shift observed in the 45°C-grown P3HT sample, therefore, suggests that its ground state is in a more regioregular conformation and has fewer regiorandom structures (fig. S1D), which is consistent with its higher thermal conductivity compared with the 85°C-grown P3HT. The 85°C-grown chains have more regiorandom structures, leading to amorphous thin film growth, which is further confirmed by the later x-ray scattering characterizations. The disordered morphology of regiorandom chains not only results in smaller thermal conductivity along the chain but also leads to larger separation and poor heat transfer between chains.

To explain the observed temperature-dependent thermal conductivity, we used synchrotron grazing incidence wide-angle x-ray scattering (GIWAXS) to investigate the nanostructures, including crystalline lattice constants and orientation information by {h00} and {0k0} scatterings (Fig. 4 and fig. S3D). The GIWAXS pattern from the 45°C-grown P3HT film shows powder scattering–like rings (Fig. 4A), suggesting a polycrystalline structure of no preferred molecular orientations with respect to the structure. This is favorable for achieving near-isotropic thermal conductivity. The {100} scattering due to the lamellar layer structure (q ~ 0.38 $Å^{-1}$) and the {010} scattering due to π-π interchain stacking (q ~ 1.6 $Å^{-1}$) are present in the 45°C-grown P3HT film, confirming the intermolecular self-assembly of regioregular sections by π-π interactions (Fig. 4A). In contrast, neither powder rings nor the {010} scattering is observed in the 85°C-grown P3HT film (Fig. 4B), suggesting that the disordered structure is dominant. Because the π-π stacking interaction is approximately 10 to 100 times stronger than the vdW forces (*21*), the observed π-π interactions along the {010} direction are expected to enable efficient thermal transport between chains. The diffuse scatterings in Fig. 4A suggest that the 45°C-grown P3HT also contains a disordered phase.

On the basis of the above structural characterization and the prediction that an individual polythiophene molecular chain has high thermal conductivity (*20*), we suggest one possible explanation for the observed high thermal conductivity in the 45°C-grown P3HT as follows. Crystalline grains formed by regioregular P3HT regions are surrounded by amorphous regions. The amorphous region has higher thermal resistance, which leads to the typical temperature dependence observed in inorganic polycrystalline materials (*35*), first increasing with temperature due to the size effect that limits the thermal conductivity of the crystalline region. At higher temperatures, the thermal resistance of the amorphous region is reduced and phonon-phonon scattering in the crystalline region starts to limit the thermal conductivity, as shown by the weak decreasing trend of thermal conductivity near 300 K.

CONCLUSIONS

In summary, we achieve a near–room temperature thermal conductivity of 2.2 W/m·K in P3HT films, which is 10 times higher than in typical polymers. In contrast to conventional efforts to enhance thermal conductivity by post-processing, such as mechanically stretching or mixing existing polymers, oCVD allows us to control both intermolecular and intramolecular structures at the molecular level during polymerization. Our thermal and structural characterizations reveal that the strong conjugated carbon-carbon double bonds along the extended polymer chains and the strong π-π stacking interactions between chains are at

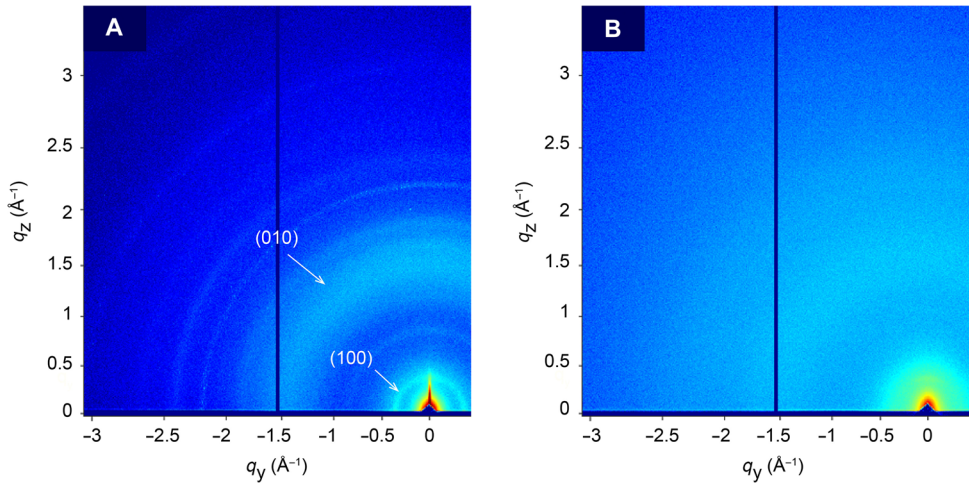

Fig. 4. Atomic-level characterization by x-ray scattering. (**A**) GIWAXS pattern of the 45°C-grown P3HT on glass substrate and characteristic Bragg scatterings by the {0k0} and {h00} plane groups are observed. The ring-shaped scattering pattern suggests that, in addition to an amorphous phase, there are crystalline regions with no preferred orientation. (**B**) GIWAXS pattern of the 85°C-grown P3HT on glass substrate suggests that the amorphous phase is dominant.

the heart of the substantially enhanced thermal transport. The non-destructive nature and conformal growth inherent to the oCVD process allow the formation of high-quality thermally conductive thin films on various substrates, demonstrating its versatility and near-universal applicability. Together with the wide range of material choice and scalability of the oCVD process, its aforementioned benefits open up new avenues toward advanced thermal management, especially in organic electronics and optoelectronics where lightweight and flexible polymeric heat conductors can be readily integrated.

MATERIALS AND METHODS

Details of the oCVD sample growth process and the thermal and structural characterizations can be found in the Supplementary Materials.

SUPPLEMENTARY MATERIALS

Supplementary material for this article is available at http://advances.sciencemag.org/cgi/content/full/4/3/eaar3031/DC1

section S1. Materials and Methods
section S2. Characterizations
table S1. Molecular weight and molecular weight distribution.
fig. S1. Synthesis mechanism and molecular structure.
fig. S2. Cartoon for P3HT backbone conformation.
fig. S3. Morphology, thickness, elemental analysis, and x-ray scattering characterization.
fig. S4. NMR spectroscopy.
fig. S5. Specific heat analysis and Raman spectroscopy.
fig. S6. Schematic of the TDTR method for thermal conductivity measurement.
fig. S7. Measured thermal conductivity for multiple samples at 300 K.
fig. S8. Temperature-dependent TDTR data.
fig. S9. TDTR sensitivity analysis.
fig. S10. TDTR uncertainty analysis.
References (*36*–*40*)

REFERENCES AND NOTES

1. M. Peplow, The plastics revolution: How chemists are pushing polymers to new limits. *Nature* **536**, 266–268 (2016).
2. L. H. Sperling, *Introduction to Polymer Science* (John Wiley & Sons Inc., 2005).
3. A. Henry, Thermal transport in polymers. *Annu. Rev. Heat Transf.* **17**, 485–520 (2014).
4. C. L. Choy, Thermal conductivity of polymers. *Polymer* **18**, 984–1004 (1977).
5. B. Poulaert, R. Legras, J. C. Chielens, C. Vandenhende, J. P. Issi, Thermal conductivity of highly oriented polyethylene fibers. *Polym. Commun.* **31**, 148–151 (1990).
6. H. Fujishiro, M. Ikebe, T. Kashima, A. Yamanaka Thermal conductivity and diffusivity of high-strength polymer fibers. *Jpn. J. Appl. Phys.* **36**, 5633–5637 (1997).
7. S. Shen, A. Henry, J. Tong, R. Zheng, G. Chen, Polyethylene nanofibres with very high thermal conductivities. *Nat. Nanotechnol.* **5**, 251–255 (2010).
8. X. Wang, V. Ho, R. A. Segalman, D. G. Cahill Thermal conductivity of high-modulus polymer fibers. *Macromolecules* **46**, 4937–4943 (2013).
9. Y. Xu, D. Kraemer, B. Song, Z. Jiang, J. Zhou, J. Loomis, J. Wang, M. Li, H. Ghasemi, X. Huang, X. Li, G. Chen, Nanostructured polymer films with metal-like thermal conductivity, https://arxiv.org/abs/1708.06416 (2017).
10. V. Singh, T. L. Bougher, A. Weathers, Y. Cai, K. Bi, M. T. Pettes, S. A. McMenamin, W. Lv, D. P. Resler, T. R. Gattuso, D. H. Altman, K. H. Sandhage, L. Shi, A. Henry, B. A. Cola, High thermal conductivity of chain-oriented amorphous polythiophene. *Nat. Nanotechnol.* **9**, 384–390 (2014).
11. M. K. Smith, V. Singh, K. Kalaitzidou, B. A. Cola Poly(3-hexylthiophene) nanotube array surfaces with tunable wetting and contact thermal energy transport. *ACS Nano* **9**, 1080–1088 (2015).
12. A. Roy, T. L. Bougher, R. Geng, Y. Ke, J. Locklin, B. A. Cola, Thermal conductance of poly(3-methylthiophene) brushes. *ACS Appl. Mater. Interfaces* **8**, 25578–25585 (2016).
13. H. Chen, V. V. Ginzburg, J. Yang, Y. Yang, W. Liu, Y. Huang, L. Du, B. Chen, Thermal conductivity of polymer-based composites: Fundamentals and applications. *Prog. Polym. Sci.* **59**, 41–85 (2016).
14. X. Xie, D. Li, T.-H. Tsai, J. Liu, P. V. Braun, D. G. Cahill, Thermal conductivity, heat capacity, and elastic constants of water-soluble polymers and polymer blends. *Macromolecules* **49**, 972–978 (2016).
15. G.-H. Kim, D. Lee, A. Shanker, L. Shao, M. S. Kwon, D. Gidley, J. Kim, K. P. Pipe, High thermal conductivity in amorphous polymer blends by engineered interchain interactions. *Nat. Mater.* **14**, 295–300 (2015).
16. L. Mu, J. He, Y. Li, T. Ji, N. Mehra, Y. Shi, J. Zhu, Molecular origin of efficient phonon transfer in modulated polymer blends: Effect of hydrogen bonding on polymer coil size and assembled microstructure. *J. Phys. Chem. C* **121**, 14204–14212 (2017).
17. A. Shanker, C. Li, G.-H. Kim, D. Gidley, K. P. Pipe, J. Kim, High thermal conductivity in electrostatically engineered amorphous polymers. *Sci. Adv.* **3**, e1700342 (2017).
18. R. J. Ouellette, J. D. Rawn, *Organic Chemistry Structure, Mechanism, and Synthesis* (Elsevier, 2014).
19. A. A. Balandin, Thermal properties of graphene and nanostructured carbon materials. *Nat. Mater.* **10**, 569–581 (2011).
20. T. Zhang, X. Wu, T. Luo, Polymer nanofibers with outstanding thermal conductivity and thermal stability: Fundamental linkage between molecular characteristics and macroscopic thermal properties. *J. Phys. Chem. C* **118**, 21148–21159 (2014).
21. E. Frieden, Non-covalent interactions: Key to biological flexibility and specificity. *J. Chem. Educ.* **52**, 754 (1975).
22. M. Wang, X. Wang, P. Moni, A. Liu, D. H. Kim, W. J. Jo, H. Sojoudi, K. K. Gleason, CVD polymers for devices and device fabrication. *Adv. Mater.* **29**, 1604606 (2017).
23. A. J. Heeger, N. S. Sariciftci, E. B. Namdas, *Semiconducting and Metallic Polymers* (Oxford Univ. Press, 2010).

24. A. M. Coclite, R. M. Howden, D. C. Borrelli, C. D. Petruczok, R. Yang, J. L. Yagüe, A. Ugur, N. Chen, S. Lee, W. J. Jo, A. Liu, X. Wang, K. K. Gleason, 25th anniversary article: CVD polymers: A new paradigm for surface modification and device fabrication. *Adv. Mater.* **25**, 5392–5423 (2013).
25. K. K. Gleason, *CVD Polymers: Fabrication of Organic Surfaces and Devices* (Wiley, 2015).
26. A. Asatekin, M. C. Barr, S. H. Baxamusa, K. K. S. Lau, W. Tenhaeff, J. Xu, K. K. Gleason, Designing polymer surfaces via vapor deposition. *Mater. Today* **13**, 26–33 (2010).
27. A. J. Heeger, Semiconducting and metallic polymers: The fourth generation of polymeric materials (Nobel Lecture). *Angew. Chem. Int. Ed.* **40**, 2591–2611 (2001).
28. D. G. Cahill, W. K. Ford, K. E. Goodson, G. D. Mahan, A. Majumdar, H. J. Maris, R. Merlin, S. R. Phillpot, Nanoscale thermal transport. *J. Appl. Phys.* **93**, 793–818 (2003).
29. A. J. Schmidt, X. Chen, G. Chen, Pulse accumulation, radial heat conduction, and anisotropic thermal conductivity in pump-probe transient thermoreflectance. *Rev. Sci. Instrum.* **79**, 114902 (2008).
30. W. C. Tsoi, D. T. James, J. S. Kim, P. G. Nicholson, C. E. Murphy, D. D. C. Bradley, J. Nelson, J.-S. Kim, The nature of in-plane skeleton Raman modes of P3HT and their correlation to the degree of molecular order in P3HT:PCBM blend thin films. *J. Am. Chem. Soc.* **133**, 9834–9843 (2011).
31. S. Nejati, K. K. S. Lau Chemical vapor deposition synthesis of tunable unsubstituted polythiophene. *Langmuir* **27**, 15223–15229 (2011).
32. I. F. Perepichka, D. F. Perepichka, *Handbook of Thiophene-Based Materials: Applications in Organic Electronics and Photonics* (Wiley, 2009).
33. J. L. Brédas, Relationship between band gap and bond length alternation in organic conjugated polymers. *J. Chem. Phys.* **82**, 3808–3811 (1985).
34. E. Busby, E. C. Carroll, E. M. Chinn, L. Chang, A. J. Moulé, D. S. Larsen, Excited-state self-trapping and ground-state relaxation dynamics in poly(3-hexylthiophene) resolved with broadband pump–dump–probe spectroscopy. *J. Phys. Chem. Lett.* **2**, 2764–2769 (2011).
35. G. Chen, *Nanoscale Energy Transport and Conversion: A Parallel Treatment of Electrons, Molecules, Phonons, and Photons* (Oxford Univ. Press, 2005).
36. A. Ugur, F. Katmis, M. Li, L. Wu, Y. Zhu, K. K. Varanasi, K. K. Gleason, Low-dimensional conduction mechanisms in highly conductive and transparent conjugated polymers. *Adv. Mater.* **27**, 4604–4610 (2015).
37. W. E. Tenhaeff, K. K. Gleason, Initiated and oxidative chemical vapor deposition of polymeric thin films: iCVD and oCVD. *Adv. Funct. Mater.* **18**, 979–992 (2008).
38. R. M. Costescu, M. A. Wall, D. G. Cahill, Thermal conductance of epitaxial interfaces. *Phys. Rev. B* **67**, 054302 (2003).
39. J. P. Feser, D. G. Cahill Probing anisotropic heat transport using time-domain thermoreflectance with offset laser spots. *Rev. Sci. Instrum.* **83**, 104901 (2012).
40. T. M. Pappenfus, D. L. Hermanson, S. G. Kohl, J. H. Melby, L. M. Thoma, N. E. Carpenter, D. A. da Silva Filho, J.-L. Bredas, Regiochemistry of poly(3-hexylthiophene): Synthesis and investigation of a conducting polymer. *J. Chem. Educ.* **87**, 522–525 (2010).

Acknowledgments: We thank T. Swager for allowing us to access nuclear magnetic resonance (NMR) and gel permeation chromatography (GPC) instruments; P. Wang and L. Moh for NMR, differential scanning calorimetry, and GPC discussions; S. Huang for Raman discussions; M. Luckyanova, L. Meroueh, and J. Tong for TDTR discussions; Z. Ding for the temperature-dependent thermal transport discussion; and J. Tong, L. Meroueh, and V. Chiloyan for the proofreading. **Funding:** We acknowledge support from the U.S. Department of Energy (DOE)–Basic Energy Sciences (Award No. DE-FG02-02ER45977) (for fundamental research on heat conduction in polymers) and Massachusetts Institute of Technology (MIT) Deshpande Center (for market studies). This research used resources of the Advanced Photon Source, a U.S. DOE Office of Science User Facility operated for the DOE Office of Science by Argonne National Laboratory under contract no. DE-AC02-06CH11357. **Author contributions:** Y.X. conceived and initiated the research, proposed the polymer structure and synthesis, characterized the molecular structures, and wrote the manuscript. X.W. fabricated the polymers and, together with Y.X., took the AFM images. J.Z., Y.X., and B.S. characterized the thermal properties. S.H. contributed to the discussion and understanding of TDTR results. E.M.Y.L., Y.X., and X.W. characterized the optical properties. Z.J. conducted the x-ray scatterings and, together with Y.X., analyzed the results. All authors discussed the results and commented on the manuscript. G.C. and K.K.G. directed the research. **Competing interests:** G.C., K.K.G., Y.X., and X.W. are inventors on a provisional patent application related to this work filed by MIT (serial no. 62/619,212, filed 19 January 2018). The other authors declare that they have no competing interests. **Data and materials availability:** All data needed to evaluate the conclusions in the paper are present in the paper and/or the Supplementary Materials. Additional data related to this paper may be requested from the authors.

Submitted 24 October 2017
Accepted 12 February 2018
Published 30 March 2018
10.1126/sciadv.aar3031

Citation: Y. Xu, X. Wang, J. Zhou, B. Song, Z. Jiang, E. M. Y. Lee, S. Huberman, K. K. Gleason, G. Chen, Molecular engineered conjugated polymer with high thermal conductivity. *Sci. Adv.* **4**, eaar3031 (2018).